Experimental Validation of a Dynamic Equivalent Model for Microgrids

Francesco Conte, Fabio D'Agostino,
Stefano Massucco, Federico Silvestro
DITEN – Università degli studi di Genova
Genova, Italy
federico.silvestro@unige.it

Claudio Bossi, Mattia Cabiati
Ricerca sul Sistema Energetico – RSE S.p.A.
Milano, Italy
mattia.cabiati@rse-web.it

***Abstract*—This paper presents the results of an experimental validation of an equivalent modeling for microgrids. The main goal is to represent, with a simplified model, the dynamic response of a microgrid, in terms of active and reactive power exchanges at the point of common coupling, to variations of voltage and frequency. A nonlinear equivalent model with operational constraints is proposed. An identification procedure is used to define model parameters. To validate the approach, a set of experimental tests have been carried out on a real LV microgrid considering different configurations. Results show the effectiveness of the proposed technique and applicability to dynamic simulations.**

Keywords—dynamic equivalents, microgrids, gray-box modeling, system identification, experimental results.

I. Introduction

During last decades, the huge installation of distributed generation (DG) has drastically transformed the electric power system. One of the most significant differences from the past is the transformation of distribution networks, which have become active components of the power system. Indeed, they include generation and many inverted-interfaced devices, which can potentially implement dynamic responses to external disturbances. To realize consistent transient stability studies, it is therefore required to include in the power system models, the dynamic behavior of active distribution networks (ADNs). This issue is highly challenging, since the distribution system is complex, extremely large, and a detailed knowledge is not always available. Therefore, to build a highly detailed model of the distribution system, to be included in the overall power system model, is not possible; moreover, it would result to be useless, since the simulation of such an extremely large model could be hard and, in any case, not compatible with real time analysis.

These considerations motivate the development of several approaches in defining equivalent models for ADNs. The idea is to derive a simplified Equivalent Dynamic Models (EDM), able to represent the dynamical response of the ADN. Recent literature proposes many different solutions [1]-[2]. Generally, *measurement-based methods* are preferred to other approaches since they do not require a detailed *a priori* knowledge of the ADN. In [3]-[4] artificial neural networks (ANNs) are used to identify EDMs for ADNs and microgrids, which can be considered as a special cases of ADNs. *Prony analysis* is applied in [5] and [6].

All mentioned methods use the so called *black-box* approach, which does not assume any pre-established form of models. Differently, in the *gray-box* approach, a model structure is selected using the available information about the ADN. Gray-box models are recommended in [2] and [7] since black-box ones require more measurements to be identified, and are less adaptable to different network configurations.

A gray-box model for ADNs is proposed in [8], and validated by simulations in [9]. An improved version is introduced in [10]. A similar approach is illustrated in [11] for grid-connected microgrids. In these papers, the proposed model is nonlinear, and the parameters identification is carried out using nonlinear optimization. In [12], a similar nonlinear model is proposed, but the identification process is made more consistent adding operational and modeling constraints, and defining a precise identification procedure that starts from the available information about the ADN. In [13], modeling constraints are included in the identification of an EDM for ADNs that includes inverter-interfaced generators.

The mentioned gray-box approaches have been validated by simulation analysis, using highly detailed models to represent the real field. In this paper, the modeling and identification method introduced in [11] for ADNs is adapted to microgrids, that implement inverter-interfaced generators and/or loads, and it is validated with experimental data. Measurements are collected from a real LV microgrid that include a synchronous generator, two batteries, a photovoltaic (PV) power plant and static loads. Different configurations, including both islanded and grid-connected operating conditions are considered. Results prove the consistency and the accuracy of the proposed method.

The paper is organized as follows. Section II recalls the modeling and identification methodology. Section III describes the experimental setup. Section IV presents results. Section V summarizes the conclusions of the paper.

TABLE I. Nomenclature

Symbol	Description
T'_{ds}	direct-axes time constant of equivalent Synchronous Machine (SM) [s]
H_s	inertia time constant of equivalent SM [s]
X_s	steady-state reactance of equivalent SM [pu]
X'_s	transient reactance of equivalent SM [pu]
T_{ms}	mechanical torque of equivalent SM [pu]
E_f	field voltage of equivalent SM [pu]
D	damping factor of equivalent SM [pu]
S_s^{nom}	nominal apparent power of equivalent SM [VA]
Ω^{nom}	nominal angular velocity of the SM [rad/s]
P_Z , Q_Z	active and reactive powers absorbed by constant impedance component of the static load [W], [var]
P_I , Q_I	active and reactive powers absorbed by constant current component of the static load [W], [var]
P_P , Q_P	active and reactive powers absorbed by constant power component of the static load [W], [var]

This work has been financed by the Research Fund for the Italian Electrical System, Italy in compliance with the Decree of April 16, 2018.

978-1-7281-7455-6/20/$31.00 ©2020 IEEE

II. METHODOLOGY

Model definition and parameters identification represent the two main tasks of the proposed methodology, whose flow chart is illustrated in Fig. 1. The model definition is obtained through the selection of a proper model frame, based on the basic *a priori* knowledge, such as the type of sources available and their rated power. The parameters identification procedure defines the values of the parameters of the EDM previously defined, starting from measurements at the microgrid point of common coupling (PCC). At the end of this procedures, the microgrid EDM is fully defined, and it can be simulated to prove the effectiveness of the entire process.

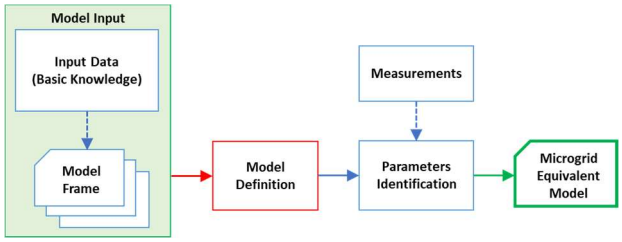

Fig. 1. Flow chart of the methodology.

A. Model Definition

The general frame of the microgrid EDM includes a ZIP load, a synchronous machine and a static source, which covers inverter driven generation, and inverter-interfaced loads. The model can potentially include an asynchronous machine [12], which is not installed in the experimental test site considered in this paper; therefore, it has not been included in this specific application. The basic system knowledge allows a first characterization of the EDM, through the proper customization of the general model frame, illustrated in the following Fig. 2.

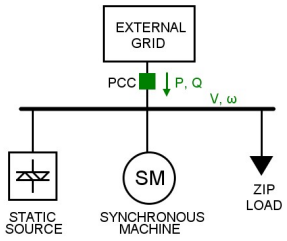

Fig. 2. General frame of the microgrid EDM.

As shown in the figure, the microgrid exchanges the active and reactive powers P [W] and Q [Var] at the PCC. Positive values mean import, negative values mean export. Moreover, V [pu] is the bus voltage and ω [pu] is the grid angular velocity (frequency) at the PCC. The principal objective of the EDM is to reproduce P and Q responses to voltage and frequency variations at the PCC.

The equivalent synchronous machine (SM) is represented with a third-order dynamic model [1]:

$$\dot{E}'_s = \frac{1}{T'_{ds}}\left(E_f - \frac{X_s}{X'_s}E'_s + \frac{X_s - X'_s}{X'_s}V\cos(\delta_s)\right) \quad (1)$$

$$\dot{\omega}_s = \frac{1}{H_s}\left(T_{ms} - \frac{V_s E'_s}{X'_s}\sin(\delta_s) - D(\omega_s - \omega)\right) \quad (2)$$

$$\dot{\delta}_s = \Omega^{\text{nom}}(\omega_s - \omega) \quad (3)$$

where: E'_s [pu] is the voltage behind the transient reactance X_s, ω_s [pu] is the machine angular velocity, δ_s is the angle between E' and V.

The ZIP load implements the dependency of load to the voltage magnitude variation for the constant impedance, current and power components. Active and reactive power exchanges of the static source depend on voltage magnitude and frequency deviations. These dependencies have been modeled with linear relations, through parameters R_P, D_P and R_Q, D_Q, in order to catch the most significant behavior of static sources, equipped with droop based controllers [14]. Therefore, the active and reactive power exchange at the PCC can be written as follows:

$$P = P_Z V^2 + P_I V + P_P + R_P V + D_P(\omega - 1) - S_s^{\text{nom}}\frac{V_s E'_s}{X'_s}\sin(\delta_s) \quad (4)$$

$$Q = Q_Z V^2 + Q_I V + Q_P + R_Q V + D_Q(\omega - 1) + S_s^{\text{nom}}\left(\frac{V E'_s}{X'_s}\cos(\delta_s) - \frac{V^2}{X'_s}\right) \quad (5)$$

B. Parameters identification

The vector θ, reported in (6), includes the entire set of parameters that has to be estimated by the identification procedure. It is composed by three subsets: vector θ_{sm}, in (7), collects the equivalent SM parameters; vectors θ_v, in (8), and θ_ω, in (9), include parameters that define the system response to voltage and frequency variations respectively, excluding the SM dynamics:

$$\theta = [\theta_{sm} \quad \theta_v \quad \theta_\omega] \quad (6)$$

$$\theta_{sm} = [T'_{ds} \quad X_s \quad X'_s \quad H_s \quad T_{ms} \quad S_s^{nom} \quad E_f \quad D] \quad (7)$$

$$\theta_v = [P_Z \quad P'_I \quad P_P \quad Q_Z \quad Q'_I \quad Q_P] \quad (8)$$

$$\theta_\omega = [D_P \quad D_Q] \quad (9)$$

In (8), $P'_I = P_I + R_P$ and $Q'_I = Q_I + R_Q$. Indeed, in (4) and (5) we can note that both the impedance constant component of the ZIP load and the static source introduce a proportional response to the voltage variation.

The measurements set used in the identification process is composes by V, ω, P, and Q at the PCC. Assuming to have a dataset composed by N samples of each quantity, the parameters estimation is obtained by solving the following nonlinear constrained optimization problem:

$$\theta^* = \min_\theta = \sum_{k=0}^{N-1}\left[\frac{(P_k - \hat{P}_{k,\theta})^2}{P_0^2} + \frac{(Q_k - \hat{Q}_{k,\theta})^2}{Q_0^2}\right] \quad (10)$$

subject to:

$$0 < T'_{ds} \le T'_{ds,\max} \quad (11)$$

$$0 < X'_s < X_s \quad (12)$$

$$0 < H_s \le H_{s,\max} \quad (13)$$

$$0 \le S_s^{\text{nom}} \quad (14)$$

$$0 < D \quad (15)$$

$$0 \le T_{ms} \le 1 \quad (16)$$

$$0 < X_s(\cos(\delta^0_{s,\max}) - E'^0_{s,\min}) + X'_s E_f - X'_s\cos(\delta^0_{s,\max}) \quad (17)$$

$$0 \le X_s(E'^0_{s,max} - 1) - X'_s E_f + X'_s \quad (18)$$

$$0 \le -X'_s T_{ms} + E'^0_{s,\max}\sin(\delta^0_{s,\max}) \quad (19)$$

In (10), P_k and Q_k are the active and reactive power k-sample of measurements, and $\hat{P}_{k,\theta}$ and $\hat{P}_{k,\theta}$ are the active and reactive power obtained by simulating the microgrid EDM, given a value for the parameter set θ.

Constraints (11)-(16) are modeling assumptions. All parameters are indeed forced to be positive, since they are defined as positive quantities. Moreover, T'_{ds} and H'_s are limited by maximum values. Constraints (17)-(19) are obtained by combining operating constraints with the steady-state equations of system (1)-(3) (the apex '0' indicates steady state values). The operational constraints are that the SM field voltage E_f is large enough to obtain that $E'^0_s > 0$, (SM working as generator), and that $0 < \delta^0_s \leq \delta^0_{s,\max}$, with $\delta^0_{s,\max} \in (0,90)$ deg.

Notice that constraints (11)-(16) are all linear with respect to the model parameters in θ_{ms}. Whereas (17)-(19) are quadratic but they can be easily transformed into linear inequalities by replacing X_s and X'_s with the auxiliary variables $\alpha_s = X_s/X'_s$ and $\alpha'_s = 1/X'_s$.

To initialize the optimization, an initial value of the model parameters should be indicated. This step is fundamental since the problem is highly nonlinear and non-convex. Thus, many local minima could exist, and a correct initialization is crucial to obtain an accurate estimation of the parameters. Initialization is carried out using all *a priori* information about the microgrid, such as the total nominal power of generators and loads. Once initialized, each parameter ϑ_i is associated to a percentage confidence interval $tol^{\%}_{\vartheta_i}$, and the following constraint is added to the optimization problem:

$$\vartheta^0_i\left(1-\frac{tol^{\%}_{\vartheta_i}}{100}\right) \leq \vartheta_i \leq \vartheta^0_i\left(1+\frac{tol^{\%}_{\vartheta_i}}{100}\right). \qquad (20)$$

The parameters identification is finally realized by solving problem (10)-(20), using a proper solver for nonlinear optimization. In this work, the "interior-point" method, implemented by the MATLAB function *fmincon*, is used.

III. Experimental Setup

In this section, we first describe the test facility used to validate the equivalent modeling approach introduced in Section II, and then we detail the experimental scenarios.

A. Test facility description

The Test Facility (TF) owned by RSE is a LV microgrid designed to perform studies and experimental tests on distributed energy resources (DERs) and smart grids methodologies [15].

The network is composed of a MV/LV transformer (800 kVA) and 6 LV feeders, that can be extended using line segments (100, 150, and 200 m length). The maximum generated power is 350kVA, plus a co-generated thermal power equal to 200kWth.

The following generators are installed on the TF: different types of PV plant (total of 25kWp), a solar-thermal plant (10kW), a micro-wind generator (2kWp), a CHP with a gas synchronous generator (50 kW), and a Diesel generator (7kVA). Moreover, there are battery energy storage systems (BESSs) (Litium, SoNick, Vanadium Redox, Lead Acid), programmable loads (resistive, inductive and capacitive), and a 400V-100kW AC/DC interface with a DC grid.

The following Fig. 3 shows the block diagram and the composition of the portion of the TF used in this study, and the three configurations adopted to generate the experimental datasets, which are detailed in the next subsection.

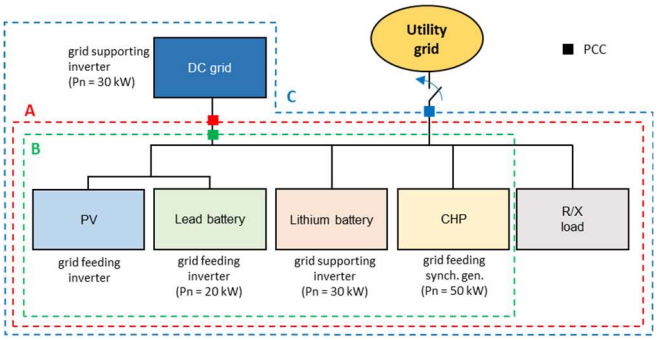

Fig. 3. Diagram of the portion of Test Facitily used in this study. Dashed lines define the aggregate which is represented by the EDM for each configuration.

B. Experimental scenarios

Three classes of configurations have been considered:

Configuration A: *TF in islanded mode with perturbations determined by the AC/DC inverter*: the portion of TF considered as the system to be identified is the one within the red box in Fig. 3, the PCC is the point of connection with the DC grid, who plays the role of external grid. The AC/DC inverter operates in "grid forming" mode [16] and imposes frequency and voltage.

Configuration B: *TF in islanded mode with load variations*: the portion of TF considered as the system to be identified is the one within the green box in Fig. 3, the PCC is the point of connection with the DC grid.

Configuration C: *TF connected to the main grid*: the portion of TF considered as the system to be identified is the one within the blue box in Fig. 3, the PCC is the point of connection with the main grid.

In all the configurations, inverters can be voltage or current controlled and they can implement equivalent droops according to the following equations [14]:

$$\Delta V = \frac{x}{\sqrt{r^2+x^2}}k_v\Delta P + \frac{x}{\sqrt{r^2+x^2}}k_v\Delta Q \qquad (21)$$

$$\Delta f = \frac{x}{\sqrt{r^2+x^2}}k_f\Delta P + \frac{r}{\sqrt{r^2+x^2}}k_f\Delta Q \qquad (22)$$

where r, x, k_v ad k_f are parameters that can be defined by the TF user.

Table II reports the details of all experimental scenarios. For each scenario, a dataset of measurements has been collected using a PMU with sampling time T_s = 0.02s. Fig. 4, Fig. 5, and Fig. 6 show three examples of datasets, one for each configuration.

IV. Results

The identification algorithm described in Section II has been applied to the datasets collected in Scenarios 1-8. In all these cases, only the first half (in terms of time) of measurements has been used for the EDM parameters identification. Two possible initial values of parameters have been used to initialize the optimization:

- **CHP out of service (Scenarios 1-2 and 5-8):** the initial conditions for the nominal power S_s^{nom} of the SM is equal to zero with a null confidence interval ($tol_{\vartheta_i}^{\%}= 0$). This means that the generator dynamics has no weight in the power exchange, and parameters to be identified are those in θ_v and θ_ω.
- **CHP in service (Scenarios 3-4)**: S_s^{nom} is initialized with 50kVA, which is the nominal power of the CHP. In this case, the confidence interval is zero since the information is exactly known. The mechanical torque T_{ms} is 0.6p.u. and null confidence interval, since in all the cases, the CHP generates 30kW. Finally, based on an estimate provided by RSE, the inertia time constant of the CHP is within the interval [0.27 0.5] s. Thus, H_s is initialized with 0.38 s with 10% of confidence.

TABLE II. EXPERIMENTAL SCENARIOS

Configuration A		
Scenario 1	Li* inverter	Voltage controlled
	Ld* inverter	Current controlled
	Virtual impedance (Li)	$r = 3,\ x = 3,\ k_f = 1,\ k_v = 5$
	CHP	Out of service
	Experiment duration	785s
Scenario 2	Li inverter	Voltage controlled
	Ld inverter	Current controlled
	Virtual impedance (Li)	$r = 3,\ x = 0, k_f = 1, k_v = 5$
	CHP	Out of service
	Experiment duration	752s
Scenario 3	Li inverter	Voltage controlled
	Ld inverter	Current controlled
	Virtual impedance (Li)	$r = 2,\ x = 5, k_f = 1, k_v = 5$
	CHP	30 kW
	Experiment duration	1623s
Configuration B		
Scenario 4	Li-Ld-DC inverters	Voltage controlled
	Virtual impedance (Li-Ld)	$r = 3,\ x = 3,\ k_f = 1, k_v = 5$
	Virtual impedance (DC)	$r = 3,\ x = 3,\ k_f = 0.1, k_v = 0.5$
	CHP	30 kW
	Load	27 kW
	Experiment duration	394s
Scenario 5	Li-Ld-DC inverters	Voltage controlled
	Virtual impedance (Li-Ld)	$r = 3,\ x = 3,\ k_f = 1, k_v = 5$
	Virtual impedance (DC)	$r = 3,\ x = 3,\ k_f = 0.1, k_v = 0.5$
	CHP	Out of service
	Load	5 kW
	Experiment duration	291s
Scenario 6	Li-DC inverters	Voltage controlled
	Ld inverter	Current controlled
	Virtual impedance (Li-DC)	$r = 3,\ x = 0,\ k_f = 0.1, k_v = 0.5$
	CHP	Out of service
	Experiment duration	935s
Scenario 7	Li-DC inverters	Voltage controlled
	Ld inverter	Current controlled
	Virtual impedance (Li-DC)	$r = 3,\ x = 3,\ k_f = 0.1, k_v = 0.5$
	CHP	Out of service
	Experiment duration	935s
Scenario 8	Li-DC inverters	Voltage controlled
	Ld inverter	Current controlled
	Virtual impedance (Li-DC)	$r = 2,\ x = 5,\ k_f = 0.1, k_v = 0.5$
	CHP	Out of service
	Experiment duration	935s
Configuration C		
Scenario 9	Li-Ld-DC inverters	Voltage controlled
	Virtual impedance (Li-Ld-DC)	$r = 3,\ x = 0,\ k_f = 1, k_v = 5$
	CHP	30kW
	Load	45kW
	Experiment duration	1623s
Scenario 10	Li-Ld-DC inverters	Voltage controlled
	Virtual impedance (Li-Ld-DC)	$r = 3,\ x = 3,\ k_f = 1, k_v = 5$
	CHP	30kW
	Load	45kW
	Experiment duration	1326s

*Li: Lithium battery, Ld: lead battery, DC: AC/DC inverter

To study the capability of the identification procedure to provide an estimate of the inertia time constant, a test on Scenario 4 has been carried out using an erroneous initialization of H_s: 5 s with a 100% confidence interval.

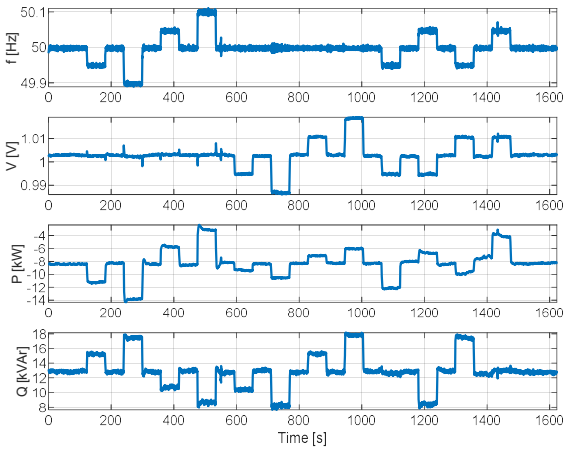

Fig. 4. Scenario 3 (Configuration A): measurements dataset

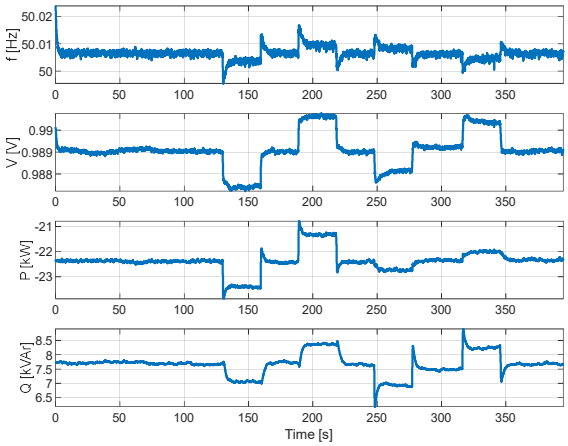

Fig. 5. Scenario 4 (Configuration B): measurements dataset.

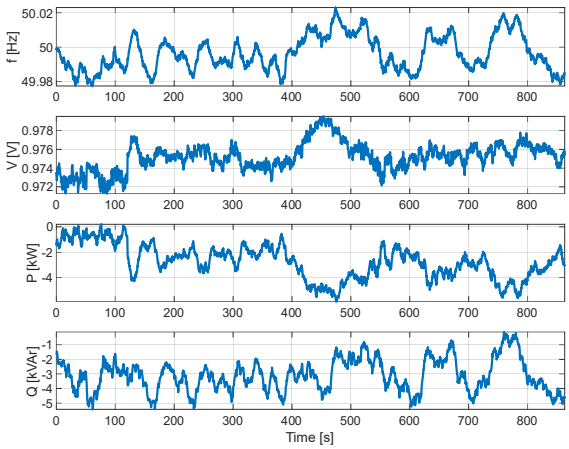

Fig. 6. Scenario 10 (Configuration C): measurements dataset.

A. Parameters indentification results

Table III and Table IV report the values of the parameters identified for scenarios 1-8. Table III is about the parameters of the static component of the model, which have been identified for all scenarios. Table IV is about the parameters of the dynamic component of the model (*i.e.* SM model), which have been identified only for scenarios 3 and 4, where the CHP is in service. As above mentioned, for Scenario 4, an identification test has been carried out using an erroneous initialization of the inertia time constant H_s. In the two tables, and hereafter in the paper, the results obtained with this erroneous initialization are indicated with "4e".

TABLE III. IDENTIFIED VALUES OF THE PARAMETERS IN θ_v AND θ_ω

Sc.	P_Z	P_I	P_P	D_P	Q_Z	Q_I	Q_P	D_Q
1	3.31	-6.39	3.07	1.98	0.00	0.20	-0.20	-2.50
2	0.00	0.30	-0.30	0.53	0.00	0.01	-0.01	-3.14
3	0.30	-0.46	0.18	2.75	0.59	-0.88	0.32	-2.27
4	0.09	0.35	-0.43	2.43	0.96	-1.44	0.51	-2.50
4e	0.09	0.32	-0.43	2.43	0.98	-1.43	0.52	-2.49
5	0.01	0.49	-0.49	1.98	0.01	0.42	-0.42	-3.14
6	0.00	0.37	-0.38	0.61	0.30	-0.58	0.28	-2.29
7	1.34	-2.40	1.06	1.44	0.00	0.27	-0.26	-1.95
8	0.07	0.01	-0.09	1.84	0.17	0.03	-0.20	-1.37

TABLE IV. IDENTIFIED VALUES OF PARAMETERS IN θ_{sm}

Sc.	D	T'_{ds}	H_s	S_s^{nom}	T_{ms}	E_f	X_s	X'_s
3	5.01	0.81	0.25	0.05	0.6	2.13	2.60	0.19
4	5.70	0.76	0.26	0.05	0.6	2.12	2.20	0.18
4e	4.75	0.72	0.20	0.05	0.6	2.15	2.49	0.11

Notice that the values of parameters of the SM identified within the different scenarios are very similar each other. This means that the identification algorithm can uniquely detect the dynamical behaviour of the CHP. However, it is worth remarking that values computed with the erroneous initialization are different with respect to the ones calculated with the correct initialization, despite they have the same order of magnitude. From the one hand, this is not surprising since the model is nonlinear, and a full identifiability cannot be obtained. On the other hand, this does not mean that the model is not able to accurately reproduce the network dynamics but that, in some scenarios, estimation of parameters cannot be precisely carried out.

B. Identification and validation results

Fig. 7 and Fig. 8 show the results of identification and validation obtained in Scenario 3 and Scenario 5, respectively. The measured profiles of P and Q are compared with the ones reproduced by the EDM. We recall that the first half (in terms of time) of the measurements is used in the identification procedure, whereas the rest is used for validation. Observing the figures, in both the scenarios, the EDM appears to be able to represent the microgrid dynamics with a good accuracy.

Power profiles in Fig. 7 and Fig. 8 are provided as examples of identification and validation results. To quantify the accuracy of the EDM in representing the system dynamics, the following root mean square errors (RMSEs) are computed:

$$\sigma_P = \sqrt{\frac{1}{N}\sum_{k=0}^{N-1}\left(P_k - \hat{P}_k\right)^2}, \quad \sigma_Q = \sqrt{\frac{1}{N}\sum_{k=0}^{N-1}\left(Q_k - \hat{Q}_k\right)^2} \qquad (23)$$

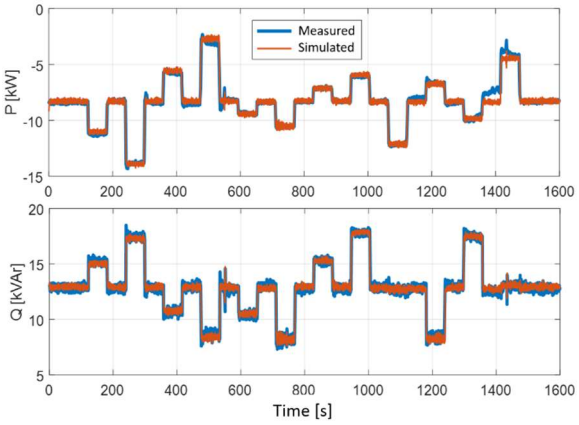

Fig. 7. Scenario 3 (Configuration A): indentification and validation results.

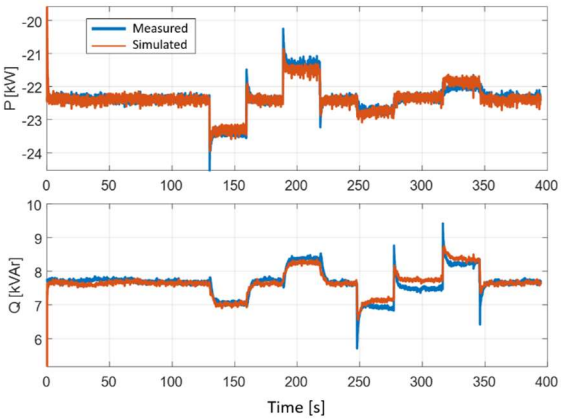

Fig. 8. Scenario 5 (Configuration B): identification and validation results.

where P_k and Q_k are active and reactive powers measured at the sampling time k, and $\hat{P}_k$ and $\hat{Q}_k$ are the active and reactive powers reproduced by the EDM, respectively.

The following Table V reports the RMSEs obtained in scenarios 1-8. Under the item "Identification", we have the RMSEs obtained with the first time half of datasets; under the item "Validation", we report the RMSEs obtained with the second time half of datasets, not used in the identification.

TABLE V. RMSES FOR IDENTIFICATION AND VALIDATION

	Identification		**Validation**	
Sc.	σ_P **[kW]**	σ_Q **[kvar]**	σ_P **[kW]**	σ_Q **[kvar]**
1	0.388	0.437	0.510	0.352
2	0.227	0.630	0.238	0.534
3	0.290	0.210	0.295	0.223
4	0.173	0.146	0.181	0.149
4e	0.180	0.145	0.183	0.152
5	0.101	0.079	0.125	0.078
6	0.109	0.114	0.171	0.125
7	0.162	0.141	0.169	0.126
8	0.221	0.134	0.212	0.126

In scenarios 3-8, RMSEs are always lower than 0.3 kW for P and 0.2 kvar for Q. In scenarios 1-2 RMSEs are lower than 0.5 kW for active power and 0.6 kvar for reactive power. This consideration holds true both for identification and validation. Since in all scenarios the order of magnitude of active and reactive power variations are in lower than 1 kW and kvar, errors can be considered to be sufficiently low, meaning that

the EDM is able to reproduce the microgrid active and reactive power responses with a good accuracy.

Also note that the difference between the RMSEs obtained in identification and validation is lower than 0.1 kW / 0.1 kvar in scenarios 1-2 and of the order of centimes of kW and kvar in scenarios 3-8. Finally observe that RMSEs obtained in scenario 4 and 4e are very close each other.

C. *Cross-validation results*

In this final part of the analysis, we evaluate the consistency and the scalability of the proposed EDM. The two EDMs identified with the dataset of Scenario 4, with correct and incorrect initializations (models 4 and 4e) have been applied to the other scenarios where the CHP is in service, *i.e.* Scenario 3 and scenarios 9 and 10. Notice that in these two last cases, differently from all other scenarios, the TF is connected to the main grid (Configuration C).

Fig. 8 shows an example of the obtained results in the case of model 4e applied to Scenario 10. Table VI reports the cross-validation RMSEs. These values are not different, in terms of order of magnitude, from the ones obtained for identification and validation (see Table V). It is therefore possible to conclude that the EDM shows a good accuracy of representation and the approach is consistent and scalable.

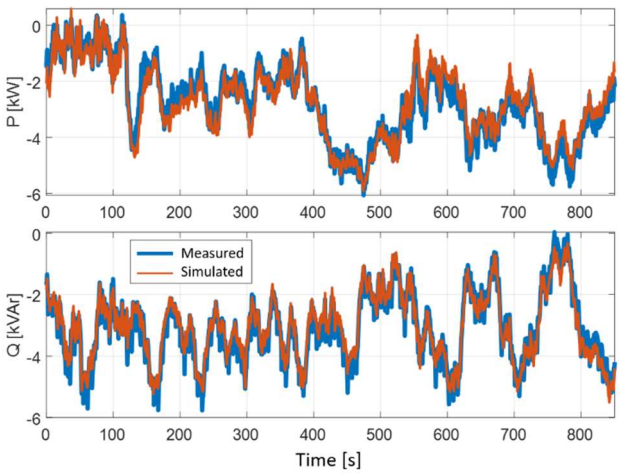

Fig. 9. Cross-validation results. Active and reactive power measured in Scenario 10 and reproduced with the EDM indentified with the dataset of Scenario 4 with erroneous initialization (EDM 4e).

TABLE VI. RMSEs FOR CROSS-VALIDATION

Scenario	Model	σ_P [kW]	σ_Q [kvar]
3	4	0.290	0.210
3	4e	0.290	0.211
9	4	0.488	0.226
9	4e	0.488	0.233
10	4	0.359	0.236
10	4e	0.356	0.235

V. CONCLUSIONS

This paper has presented the results of experimental tests carried out on a real LV microgrid, to validate an equivalent modelling and identification technique. The proposed model is nonlinear, and it is associated to a set of operational and modelling constraints. Model parameters are identified by applying a suitably developed procedure and using the real measurements of voltage, frequency and active and reactive power collected from the LV microgrid. Different configurations of the system have been considered.

Results show that the proposed equivalent model is able to accurately reproduce the dynamic response of the microgrid to external disturbances, and that it can be adapted without difficulties to different configurations. The use of this Gray-box approach allows the use of this EDM to be included in other simulation tools.

REFERENCES

[1] J.V. Milanovic *et al*, "Modelling and aggregation of loads in flexible power networks," Cigré Working Group C4.605, 2014.

[2] F.O. Resende, J. Matevosyan, and J.V. Milanovic, "Application of dynamic equivalence techniques to derive aggregated models of active distribution network cells and microgrids," in: 2013 IEEE PowerTech, Grenoble, France, 2013.

[3] C. Changchun, W. Min, D. Lihua, D. Zhixiang, and Zh. Jianyong, "Microgrid dynamic modeling based on RBF artificial neural network," in Proc. Int. Conf. Power Syst. Technol., 2014, pp. 3348–3353.

[4] A. M. Azmy, I. Erlich, "Identification of dynamic equivalents for distribution power networks using recurrent ANNs," in Proc. IEEE PES Power Systems Conf. Expo., 2004, pp. 348–353.

[5] S. M. Zali, J. V.Milanovic, "Dynamic equivalent model of distribution network cell using Prony analysis and nonlinear least square optimization," in: Proc. IEEE Power Tech, Bucharest, Romania, 2009.

[6] P. N. Papadopoulos, T. A. Papadopoulos, P. Crolla, A. J. Roscoe, G. K. Papagiannis, and G. M. Burt, "Measurement-based analysis of the dynamic performance of microgrids using system identification techniques," IET Gener., Transmiss. Distrib., vol. 9, no. 1, 2015, pp. 90–103.

[7] U.D. Annakkage *et al,* "Dynamic system equivalents: a survey of available techniques, IEEE Trans. Power Del., vol. 27, no. 1, 2012, pp. 411–420.

[8] J. V. Milanovic and S. Mat Zali, "Generic model of active distribution network for large power system stability studies," IEEE Trans. Power Syst., vol. 28, no. 3, Aug. 2013, pp. 3126–3133.

[9] J. V. Milanovic and S. Mat Zali, "Validation of equivalent dynamic model of active distribution network cell," IEEE Trans. Power Syst., vol. 28, no. 3, Aug. 2013, pp. 2101–2110.

[10] F. Conte, F. D'Agostino, S. Massucco, G. Palombo, F. Silvestro, C. Bossi, M. Cabiati, "Dynamic equivalent modelling of active distribution networks for TSO-DSO interactions," IEEE ISGT Europe 2017, Torino, Italy, 2017.

[11] B. Zaker, G. B. Gharehpetian, M. Karrari, "A Novel Measurement-Based Dynamic Equivalent Model of Grid-Connected Microgrids," in IEEE Trans. Ind. Inf., vol. 15, no. 4, 2019, pp. 2032-2043.

[12] F. Conte, F. D'Agostino, F. Silvestro, "Operational constrained nonlinear modeling and identification of active distribution newtorks,", Electric Power System Research (EPSR), vol. 168, 2019, pp. 92-104.

[13] G. Chaspierre, P. Panciatici, T. Van Cutsem, "Aggregated Dynamic Equivalent of a Distribution System Hosting Inverter-Based Generators," in: 2018 PSCC, Dublin, Ireland, 2018.

[14] K. De Brabandere, B. Bolsens, J. Van De Keybus, A. Woyte, D. J. e B. R., "A voltage and frequency droop control method for parallel inverters," IEEE Transactions on Power Electronics, vol. 22, n. 4, 2007, pp. 1107-1115.

[15] F. D'Agostino, S. Massucco, F. Silvestro, C. Bossi, A. Guagliardi, C. Sandroni, "Implementation of a distribution state estimation algorithm on a low voltage test facility with distributed energy resources," in: IEEE PES ISGT-Europe, Ljubljana, Slovenia 2016.

[16] J. Rocabert, A. Luna, F. Blaabjerg e P. Rodriguez, "Control of Power Converters in AC Microgrids," IEEE Transactions on Power Electronics, vol. 27, n. 11 , 2012, pp. 4734-4749